Inorganic Chemistry Communications 182 (2025) 115613

Contents lists available at ScienceDirect

Inorganic Chemistry Communications

journal homepage: www.elsevier.com/locate/inoche

Research Article

Multifunctional $Zn_2Ti_3O_8$ nanoparticles: Dual photocatalytic and antibiofilm activity against *Klebsiella pneumoniae*

Mohammad Reza Saadati-Gullojeh [a,1], Matin Valipour Motlagh [b,c,1], Mojgan Ghanbari [a], Amar Yasser Jassim [d], Forat H. Alsultany [e], Ayad F. Alkaim [f], Mohammad Reza Rahimi [b,c], Masoud Salavati-Niasari [a,*], Azad Khaledi [b,c,**]

[a] Institute of Nano Science and Nano Technology, University of Kashan, P.O. Box 87317-51167, Kashan, Islamic Republic of Iran
[b] Infectious Diseases Research Center, Kashan University of Medical Sciences, Kashan, Iran
[c] Department of Microbiology and Immunology, Faculty of Medicine, Kashan University of Medical Sciences, Kashan, Iran
[d] Department of Marine Vertebrate, Marine Science Center, University of Basrah, Iraq
[e] Department of Medical Physics, College of Sciences, Al-Mustaqbal University, 51001, Babylon, Iraq
[f] Department of Chemistry, College of Sciences for Women, University of Babylon, Iraq

ARTICLE INFO

Keywords:
$Zn_2Ti_3O_8$ nanostructures
Anti-biofilm
Nano-photocatalyst
Antibacterial
MTT assay
MrkA - Klebsiella Pneumoniae

ABSTRACT

In this work, the antimicrobial, antibiofilm, and photocatalyst activities of zinc titanate ($Zn_2Ti_3O_8$) nanoparticles prepared by a facile and low-cost Pechini process are reported. The antibacterial activity was evaluated against *Klebsiella pneumoniae* isolates from ICU patients, including extended-spectrum β-lactamase (ESBL)-producing isolates, by the broth microdilution method. $Zn_2Ti_3O_8$ nanoparticles exhibited potent antimicrobial activity with an MIC value of 39.06 to 156.25 μg/mL and were found to effectively inhibit biofilm formation by 69.39 % at MIC and 55.48 % at ½ MIC concentrations. Antimicrobial gene expression studies of biofilm-related genes revealed that $Zn_2Ti_3O_8$ downregulated *mrkA* gene expression 34.36 ± 1.63 % at MIC and 27.86 ± 2.49 % at ½ MIC concentrations. MTT assay cytotoxicity on HDF cell lines confirmed good biocompatibility in the antibacterially efficacious doses, with cell viability above 96 % ± 1.5 at concentrations up to 312.5 μg/mL, and a significant reduction only at higher concentrations (625 and 1250 μg/mL). At the same time, the visible light-induced photocatalytic performance of $Zn_2Ti_3O_8$ was examined with various organic dyes. The nanoparticles exhibited excellent degradation activity, especially towards methylene blue (MB), with 98.02 % degradation within 90 min. The photocatalytic performance was affected by operating conditions such as dye concentration, catalyst loading, and the presence of reactive oxygen species scavengers. Kinetic investigations established that the degradation was pseudo-first-order in nature, and the material could be reused for five cycles without any noticeable loss of activity. These results highlight the novelty of integrating antimicrobial, antibiofilm, and photocatalytic properties into a single $Zn_2Ti_3O_8$ nanomaterial, directly addressing challenges in infection control and water purification. These findings demonstrate that $Zn_2Ti_3O_8$ nanoparticles display strong multifunctional properties of effective photocatalytic degradation of contaminants, superior antibacterial and antibiofilm performances, and minimal cytotoxicity. These properties render $Zn_2Ti_3O_8$ an excellent candidate for integrated environmental and biomedical applications, with the suggestion of further in vitro and in vivo validation.

1. Introduction

Nosocomial infection caused by drug-resistant pathogens is a serious global public health problem, especially in intensive care units (ICUs) [1]. Biofilm-related infections are associated with more than 60 % of bacterial infections, and they are difficult to eradicate, which results in longer hospitalization duration, increased mortality rates, and high healthcare expenses [1]. Significant hospital pathogen *Klebsiella pneumoniae* is one of the Gram-negative bacteria that can produce strong biofilm on medical devices. Due to its swift development of resistance to

* Corresponding author.
** Corresponding author at: Infectious Diseases Research Center, Kashan University of Medical Sciences, Kashan, Iran.
E-mail addresses: salavati@kashanu.ac.ir (M. Salavati-Niasari), azadkh99@gmail.com (A. Khaledi).
[1] These authors contributed equally on this work.

https://doi.org/10.1016/j.inoche.2025.115613
Received 11 August 2025; Received in revised form 21 September 2025; Accepted 29 September 2025
Available online 10 October 2025

various antibiotics (including carbapenems), it is one of the most - dangerous priority pathogens [2].

With the decline in efficacy of traditional antibiotics, other therapeutic approaches are urgently required. One such strategy is a nanoparticle-based approach, namely, metal oxide nanoparticles showing combined antimicrobial modes such as disruption of bacterial cell membranes, prevention of bacterial biofilm, and release of ROS [3]. Nanoparticles do not cause resistance the way antibiotics do, and since they're physical, rather than chemical agents, they do not lose effectiveness with frequent use [4]. TiO_2 and ZnO nanoparticles have been extensively investigated for their antibacterial and antibiofilm performance as they are of nanoscale size, possess high surface area, and can generate ROS if subjected to specific conditions [5–8].

Zinc-titanium-based oxide materials (Zn-Ti-O), especially $Zn_2Ti_3O_8$, have been given much attention for their multiple functions. Despite their multiple applications (paint pigments [9], dielectric materials [10], humidity sensors [11], gas sensors [12]), their antibacterial and antibiofilm potential continues to be under-investigated [13]. $Zn_2Ti_3O_8$ is a kind of compound material and it not only inherits the good properties from ZnO and TiO_2 simultaneously, can also promotes the antimicrobial activity against a resistant pathogen such as *K. pneumoniae*. It is very interesting to assess the competitive index for biofilm production and expression of the virulence gene (i.e., *mrkA*) in this regard.

Besides the biomedical applications, metal oxide NPs, including TiO_2, ZnO, and their composites, have become notably efficient photocatalysts for environmental cleaning [14,15]. The efficiency of such nanomaterials is highly dependent on their thermal history, as heating and cooling profiles can significantly influence phase stability, morphology, and surface properties [16]. Such materials can utilize UV- or visible-light to produce reactive species that destroy organic pollutants (dyes, pharmaceuticals, microbial contaminants) in water sources [17]. Because of their special crystal and electronic configuration, $Zn_2Ti_3O_8$ nanoparticles show superior activity for either antimicrobial or photocatalytic purposes. The antimicrobial nature of these fabrics serves not only the purpose of fighting hospital-acquired infections but also helps against the worldwide water pollution problem.

We speculate that $Zn_2Ti_3O_8$ nanoparticles (characterized by distinctive crystal and electronic structure and the fact that they are composed of two different materials, ZnO and TiO_2) can behave as multifunctional materials exhibiting strong antibacterial/antibiofilm effects against drug-resistant pathogens and excellent photocatalytic behavior under visible light. To evaluate this hypothesis, $Zn_2Ti_3O_8$ nanoparticles were synthesized and characterized in detail to confirm the anticipated structural and optical properties. Their antibacterial and antibiofilm effects were investigated and introduced to therapeutic relevance using clinical isolates of *K. pneumoniae* (particularly with respect to biofilm inhibition and downregulation of the mrkA virulence gene). In parallel, photocatalytic degradation of organic dye pollutants was studied under visible light to evaluate their potential for environmental remediation. The rationale of this dual approach was to provide a scientific example of how $Zn_2Ti_3O_8$ provided an integrative approach to address present scientific knowledge gaps and incorporate biomedical and environmental efficacy through a singular nanomaterial.

2. Materials and methods

This section provides a detailed description of the synthesis procedure of $Zn_2Ti_3O_8$ nanoparticles using the Pechini process, along with the characterization techniques employed to analyze their structural, morphological, and functional properties. In addition, the antibacterial, antibiofilm, and photocatalytic assays conducted to evaluate their multifunctional performance are outlined.

2.1. Materials

Tetraethyl orthotitanate +98 % (TEOTi: $(C_2H_5O)_4Ti$), Ethylene glycol 35 % (EG), Citric acid ≥99 % ($C_6H_8O_7$), Ethanol 99 % (C2H5OH), Zinc nitrate hexahydrate 98 % $Zn(NO_3)_2$.6H2O, McConkey agar, RNA extraction kit, Mueller Hinton agar, crystal violet (CV), phosphate-buffered saline (PBS), methylene blue (MB), rhodamine B (RhB), methyl orange (MO), benzoic acid 99.9 % (BA), Ethylenediaminetetraacetic acid 99 % (EDTA), and 1,4-Benzoquinone 98 % (BQ), were purchased from Merck and applied as arrived without purification.

2.2. Fabrication of $Zn_2Ti_3O_8$ nanostructures

$Zn_2Ti_3O_8$ nanostructures was fabricated according to our previous work [18]. The modified Pechini procedure was performed employing Ti and Zn precursors in a 3:2 M ratio to acquire $Zn_2Ti_3O_8$. 714 mg (2.4 mmol) of $Zn(NO_3)_2$ was dissolved in 3.6 mL ethanol. 504 mg of citric acid as a chelating agent was dissolved in 3.6 mL ethanol in a separate beaker. The citric acid solution was added to $Zn(NO_3)_2$ solution and mixed for 30 min at room temperature (pH ≈ 5.5). 756 μL (3.6 mmol) of TEOTi was added to 4.8 mL ethanol and put in an ice bath ($T = 0$ °C) to control hydrolysis. The Zn–citric acid solution was added to TEOTi solution dropwise and mixed for 0.5 h in the ice bath to ensure homogeneous chelation. After that, 133.2 μL (1.2 mmol) ethylene glycol was introduced as a polymerization agent, maintaining a citric acid: ethylene glycol molar ratio of 2:1, and agitated for 20 min. The mixture was then gradually heated to 100–120 °C until solvent evaporation and gel formation occurred. The resulting gel was aged at 50 °C for 24 h, dried, and finely ground. Finally, the obtained powder was calcined at 700 °C for 6 h in ambient air with a heating rate of 5 °C/min, yielding crystalline $Zn_2Ti_3O_8$ nanoparticles. It is well established that the thermal profile during calcination and subsequent cooling significantly affects the final structure and properties of the synthesized materials [19].

2.3. Bacterial strains and culture conditions

The study comprised ten clinical isolates of *K. pneumoniae* from wound infections. The isolates have been recognized using typical biochemical procedures. For biofilm tests and gene expression experiments, the cultures were incubated overnight in Luria Bertani (LB) broth at 37 °C.

2.4. Determination of minimum inhibitory concentration (MIC)

The microdilution of the broth according to CLSI (M07-A11, 2018) was used to determine the minimum inhibitory concentrations (MICs) of TiO_2, ZnO and ZnO_2Ti_3O nanoparticles against clinical isolates of *Klebsiella pneumoniae*. Mueller-Hinton broth (MHBS) was used as a growth medium. Fresh suspension nanoparticles were prepared in sterile distilled water and sonicated for 15 min to ensure that they were free from aggregation. Two-step dilutions were then prepared on sterile 96-well plates, yielding a final concentration of 2500 to 19.53 μg per ml. The bacterial inoculum was obtained from overnight cultures grown at 37 °C on blood agar. The colonies were suspended in sterile saline and conditioned to a standard of 0.5 McFarland (1 × 10.0 CFU per ml). The suspension was then diluted with 1:150 of MHB to obtain a final inoculum in each well of approximately 5×10^5 CFU per ml. Appropriate controls included: wells with only broth (negative sterility control), bacterial suspensions with nanoparticles (positive growth control), and nanoparticles with broth and no bacteria (nanoparticle-free sterilisation control) [20].

The plates were incubated under aerobic conditions at 37 °C for 20 h. After incubation, the growth of the bacteria was assessed visually and by measuring the 600 nm optical density (OD_6) by microplate reader (BioTek, USA) using a scanner. MIC was defined as the lowest concentration of nanoparticles that completely inhibited visible growth and resulted in OD of less than 0.05 compared to the negative control. Each MIC determination was performed using three biological replicates (independent bacterial cultures) and three technical replicates (well-formed wells in the same test). The results shall be given as mean ± standard deviation (SD) [21].

2.5. Evaluation of biofilm formation

The effect of TiO_2, ZnO, and $Zn_2Ti_3O_8$ nanoparticles on the formation of biofilms by *Klebsiella pneumoniae* was assessed by a 96-well microtiter plate assay with crystal violet staining. Overnight bacterial cultures were diluted 1:100 in fresh tryptic soy broth, and 200 μL of the diluted culture was inoculated into each well. Nanoparticles were applied at concentrations of MIC and ½MIC, and the plates were incubated for 24 h under static conditions at 37 °C to allow biofilm formation.

Negative control wells contained uninoculated medium, and all experiments included three biological and three technical replicates. Following incubation, non-adherent cells were removed by washing with phosphate-buffered saline (PBS), and the remaining biofilms were fixed with 99 % methanol for 15 min. The wells were then air-dried, stained with 0.1 % crystal violet for 30 min [22]., and excess stain was removed. The bound dye was dissolved in 30 % acetic acid, and absorbance was measured at 570 nm to quantify biofilm biomass.

Biofilms treated with $Zn_2Ti_3O_8$ nanoparticles were compared to untreated control biofilms, and the percentage of biofilm inhibition was calculated using the following equation:

[1 − (A570 of treated cells / A570 of untreated control cells)] × 100

2.6. Evaluating mrkA gene expression in K. pneumoniae by real-time PCR

Total RNA was extracted from *Klebsiella pneumoniae* isolates using the RNX-Plus kit (PARSTOUS, Iran) according to the manufacturer's instructions. RNA quality and integrity were assessed using a NanoDrop spectrophotometer and 1.5 % agarose gel electrophoresis. To remove potential genomic DNA contamination, samples were treated with RNase-free DNase I.

cDNA synthesis was performed using a cDNA Synthesis Kit (PARSTOUS, Iran), and 5 ng of cDNA was used in each real-time PCR reaction. Gene expression of the mrkA gene was analyzed using specific primers and the 16 s rRNA gene as an internal control (Table 1). Reactions were performed on the ABI-X Plus system using a SYBR Green kit. The thermal cycling program included an initial denaturation at 95 °C for 15 min, followed by 35 cycles of 95 °C for 30 s and 60 °C for 60 s.

All experiments were conducted using triplicate measurements, including biological and technical replicates. The relative expression of mrkA was calculated using the ΔΔCt method, and results are expressed as mean ± SD. Statistical analyses were performed using one-way ANOVA followed by Tukey's post hoc test to determine significance, with $p < 0.05$ considered statistically significant.

2.7. Determination of nanoparticle cytotoxicity (MTT)

The biocompatibility of zinc, titanium dioxide, and zinc-titanate nanoparticles was assessed by the MTT (3-(4,5-dimethylthiazol-2-yl)-2,5-diphenyltetrazolium bromide) assay. Human dermal fibroblasts (HDFs) were obtained from the Iranian Biological Resources Center (IBRC, Iran) and used within passages 4–8. Cells were seeded in 96-well plates at a density of 10,000 cells per well and allowed to adhere overnight.

Nanoparticles were serially diluted to concentrations ranging from 19.53 to 1250 μg/mL and added to the wells for 24 h. Wells containing only culture medium were used as untreated controls. All experiments included three biological replicates, each with three technical replicates [23].

After treatment, the medium was removed, and MTT solution (0.5 mg/mL in culture medium) was added to each well. Viable cells metabolically reduced MTT into insoluble purple formazan crystals, which were subsequently dissolved for absorbance measurement at 570 nm. Cell viability was calculated as a percentage of the untreated control. Results were expressed as mean ± standard deviation (SD), and statistical analysis was conducted by means of an ANOVA with post hoc comparisons.

Cell viability (%) = (Absorbance of sample /Absorbance of control) × 100

2.8. Photocatalytic process

The $Zn_2Ti_3O_8$ photocatalyst was used under visible light irradiation to remove methylene blue, rhodamine B, and methyl orange dye. For all experiments, 50 mg of catalyst (equivalent to 0.5 mg/mL) was dissolved in 100 mL of 10 ppm dye (10 mg L^{-1}). Tests were performed in a cylindrical Pyrex glass reactor fitted with a water jacket to keep the reaction temperature at 25 ± 1 °C. A 400 W Osram visible light lamp (400–780 nm; light intensity ≈ 100 mW cm^{-2} at the surface of reactor) was used as a visible light source at a distance of 30 cm from the suspension. The reaction mixture of catalyst and dye was stirred in the dark for 30 min prior to illumination to allow for adsorption and desorption equilibrium on the catalyst surface. After stirring in the dark, 3 mL samples were taken from the reaction mixture every 15 min for 75 min, filtered through a 0.22 μm membrane to remove catalyst particles, and analyzed by UV–Vis spectrophotometry to determine the amount of dye degraded. Dye degradation was confirmed to be a result of photocatalytic activity engaging the catalyst, as all dye treatments, including the dye solutions without catalyst (light only control), the dye mixture with catalysts resting during the dark (dark control), and the dye solution without any catalyst or illumination (blank), were carried out under the same experimental conditions to confirm that dye degradation originated solely from photocatalytic activity. The decolorization efficiency (D) was determined based on the absorbance values before (A_0) and after (A_t) light exposure [24].

$$D(\%) = \frac{A_0 - A_t}{A_0} \times 100 \quad (1)$$

3. Results and discussion

In this section, the physicochemical properties of the synthesized nanoparticles are presented and discussed, followed by the evaluation of their antibacterial, antibiofilm, and photocatalytic activities. Comparative analysis with previous reports is also included to highlight the novelty and significance of our findings.

3.1. Characterization of nanoparticles

Fig. 1a shows the X-ray diffraction (XRD) pattern of $Zn_2Ti_3O_8$. The

Table 1
The primer sequences used in this study.

Target gene	Sequence primer (5′ → 3′)	Amplication size (bp)	Annealing temperature
mrkA	F 5-GCCCATGCAGCTGATACCACT-3	21	56 °C
	R 5´-TATCCGCTGCTGCCGCTT-3’	18	
16 SrRNA	F 5-ACCGCATAACGTCGCAAGACC-3	21	60 °C
	R 5´-TCCTCTCAGACCAGCTAGGGATCG-3’	24	

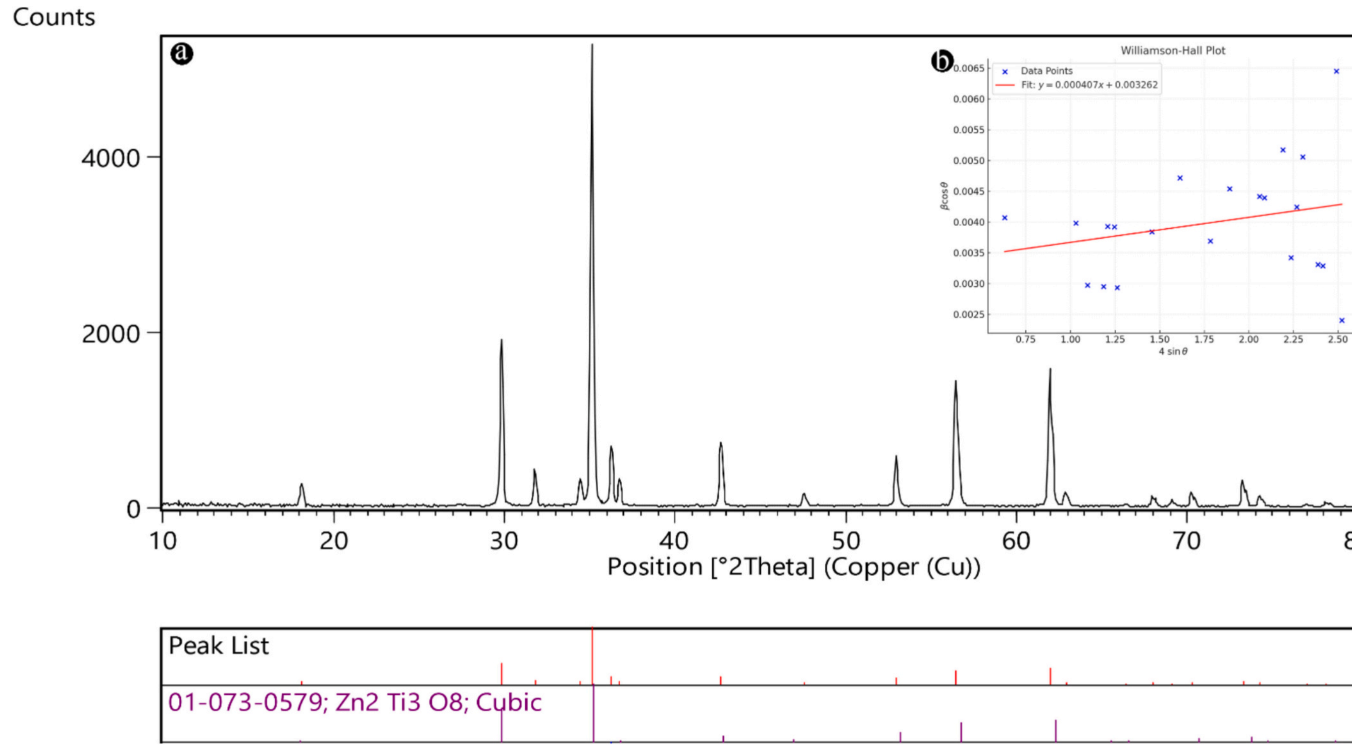

Fig. 1. a) XRD pattern and b) Williamson-Hall plot of $Zn_2Ti_3O_8$ nanostructures.

peak list provides reference data for $Zn_2Ti_3O_8$ in the cubic crystal structure (PDF card: 01–073-0579) with space group of Fd-3 m. The absence of additional significant peaks suggests that the sample is primarily composed of $Zn_2Ti_3O_8$ without significant impurities or secondary phases. The crystallite size of $Zn_2Ti_3O_8$ was calculated by Scherrer and Williamson-hall methods.

$$D = \frac{K\lambda}{\beta\cos\theta} \tag{2}$$

$$\beta\cos\theta = \frac{K\lambda}{D} + 4\varepsilon\sin\theta \tag{3}$$

In Eq. (1), K is the Bragg constant (0.9), "β" is the FWHM value, and λ denotes the X-ray wavelength (1.54 Å). In addition, crystallite size was estimated using Williamson-hall plots (Eq. 2) to study microstructural properties. ε symbolizes the microstrain. Graphing βcosθ versus sinθ allows us to derive crystallite size (Kλ/D = intercept) and strain component from the slope. The Scherrer and Williamson-hall techniques yielded crystallite sizes of 36.5 and 42.5 nm. The microstrain was likewise evaluated as 0.00041. The crystallite size determined by the Scherer equation is smaller than the crystallite size suggested by the Williamson-Hall plots, which are shown in Fig. 1b due to non-zero residual tension.

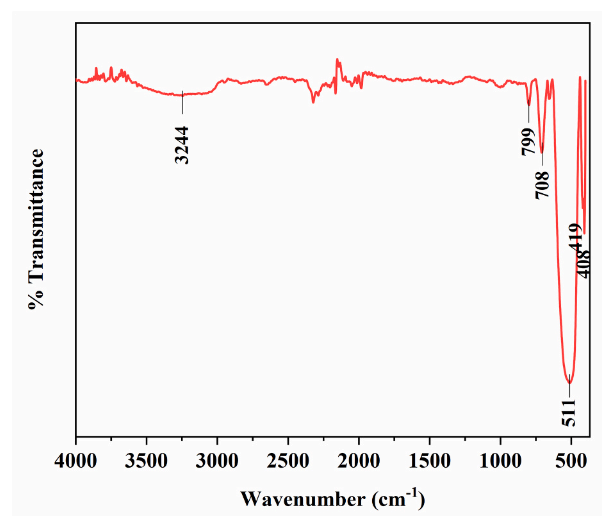

Fig. 2. FTIR spectrum of $Zn_2Ti_3O_8$ nanostructures.

Fig. 2 reveals the FTIR spectrum of $Zn_2Ti_3O_8$. Zn—O bond stretching is associated with the peak at 419 cm^{-1}, whereas Ti—O bond stretching is associated with the peak at 511 cm^{-1} [25]. Due to the tensile vibration of the water-absorbing O—H bond on the sample surface, the samples exhibit absorption maxima around 3444 cm^{-1} [26]. The Zn–O–Ti vibrational mode, was detected as a band at 708 cm^{-1} [27]. Furthermore, the vibrational mode of O–Ti–O stretching in $[TiO_6]^{2-}$ octahedral was identified as the wide band in the 799 cm^{-1} area, which was in excellent accord with the published literature [28].

Fig. 3a and b reveal the SEM images of $Zn_2Ti_3O_8$ at two different magnifications of 100 and 200 kx. These are the agglomerated particles that possess irregular morphologies. Generally, the nanoparticle size observed is of nanometer range order since some rough texture can also be viewed within the nanostructure. Larger ones are also distributed, probably showing grain boundary or agglomeration. These nanostructures of $Zn_2Ti_3O_8$ are mostly spherical, with slight aggregations. Such morphologies are normally obtained in materials prepared by the sol-gel method since nanocrystals are apt to agglomerate in the drying and calcination processes. The TEM images of $Zn_2Ti_3O_8$ in two different scales (100 nm and 20 nm) are illustrated in Fig. 3c and d. The TEM images comfirmed the morphology and the results obtained by FESEM images.The average diameter of nanoparticles was estimated to be 80.0 nm by Digimizer software.

The nitrogen adsorption–desorption isotherm (BET) showed type IV isotherm with a clear hysteresis loop, indicating the existence of a mesoporous structure (Fig. 4a). The specific area, calculated from the BET method, was 16.91 m^2 g^{-1}, which enhances the active surface for

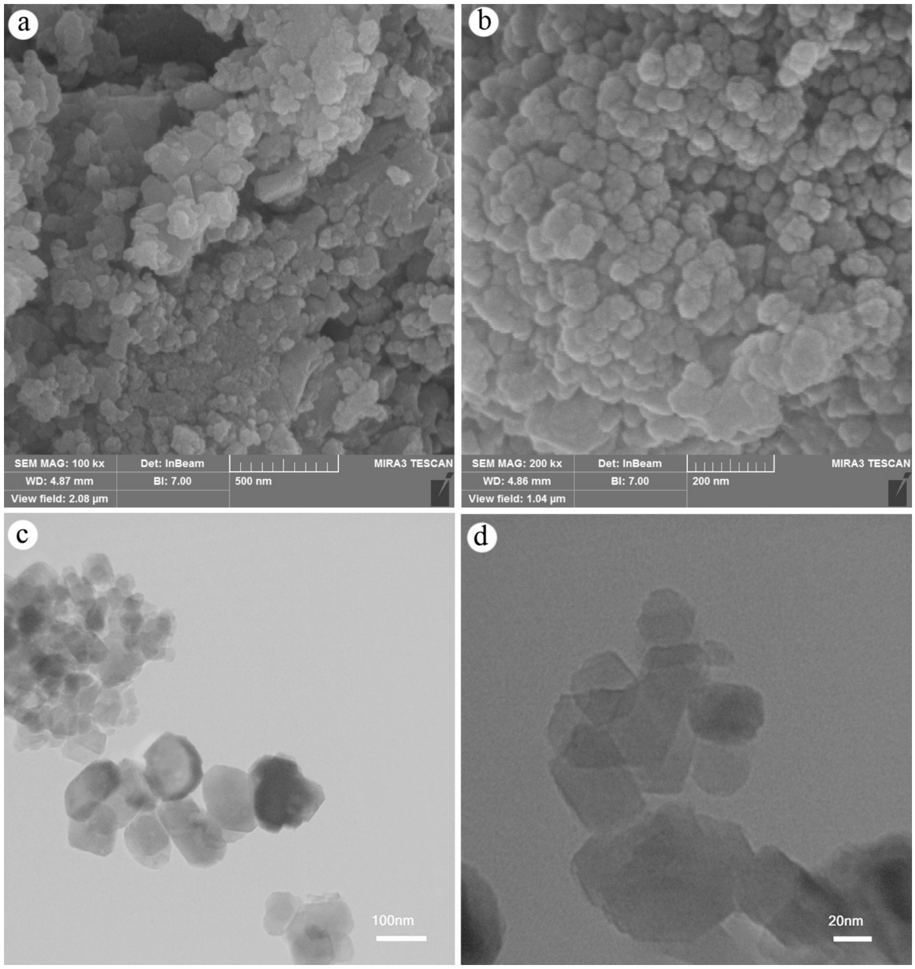

Fig. 3. (a and b) FESEM and (c and d) TEM images of of $Zn_2Ti_3O_8$ nanostructures.

photocatalytic reactions and adsorption. The average pore diameter and total pore volume (p/p0 = 0.921) were 9.054 nm and 0.01564 $cm^3\ g^{-1}$, respetivley. The BJH pore size distribution characterized the material as mesoporous with most pores in the range of 2–50 nm (Fig. 4b). The pore structure facilitates mass transfer and increases photocatalytic efficiency by the existence of available pathways for reactant diffusion.

Diffuse reflectance spectroscopy (DRS) was employed to measure the optical band gap of the $Zn_2Ti_3O_8$ composite. From Kubelka–Munk function and Tauc plot, band gap energy was found to be approximately 2.3 eV (Fig. 4d), indicating that the material is visible-sensitive. This optical property suggests that $Zn_2Ti_3O_8$ is activatable under visible light and potentially useful for photocatalytic applications.

Photoluminescence (PL) spectroscopy was employed to study the recombination rate of the photogenerated electron–hole pairs. The PL spectrum (Fig. 4e) showed an emission peak in the range of 400–500 nm, with relatively low intensity. This low emission intensity reflects a reduced recombination rate, which is desirable for the optimization of photocatalytic efficiency of the material.

3.2. Bacterial strains

In this study, ESBL (extended-spectrum beta-lactamase) producing bacterial isolates and NON- ESBL isolates were examined. Out of 44 *Klebsiella pneumoniae* isolates, 35 were of the ESBL type.

3.3. Antibiotic susceptibility testing

In this study, all clinical strains were resistant to ceftriaxone, meropenem, cefazolin, cefotaxime, cephalothin, and piperacillin-tazobactam. The antibiotic resistance pattern is listed in Table 2.

3.4. MICs of nanoparticles

The MIC of the nanoparticles was determined against *Klebsiella pneumoniae* isolates from ESBL and non-ESBL strains. $Zn_2Ti_3O_8$ nanoparticles showed the strongest antimicrobial activity, with MIC values of 156.25 ± 8, 78.12 ± 4, and 39.06 ± 2 µg/mL across the tested isolates. In contrast, ZnO and TiO_2 nanoparticles exhibited significantly higher MICs of 312.5–1250 µg/mL with approximate SDs of ±15–60 µg/mL, demonstrating lower antimicrobial efficacy compared with zinc-titanate nanoparticles (Table 3). MICs were described as the lowest nanoparticle concentrations that completely inhibited visible bacterial growth and reduced OD_{600} to $\leq$0.05 relative to growth controls. All measurements were performed in triplicate, including three biological replicates and three technical replicates and the results were reported as mean ± SD. These findings clearly show that zinc-titanate nanoparticles are more effective than zinc or titanium nanoparticles at inhibiting *K. pneumoniae* growth at significantly lower concentrations, which highlights their potential as powerful antimicrobials. The MIC_{50} and MIC_{90} values of $Zn_2Ti_3O_8$ nanoparticles against clinical isolates of *K. pneumoniae* were both 156.25 µg/mL, indicating uniform and potent antimicrobial activity across the tested strains. In this study, MBC was not established, as the focus was mainly on MIC, biofilm inhibition and analysis of gene expression. Future studies are recommended to assess MBC values and provide a more comprehensive evaluation of the antibacterial activity of nanoparticles of Zn_2Ti_3O. Venkatasubbu et al. examined the mechanisms

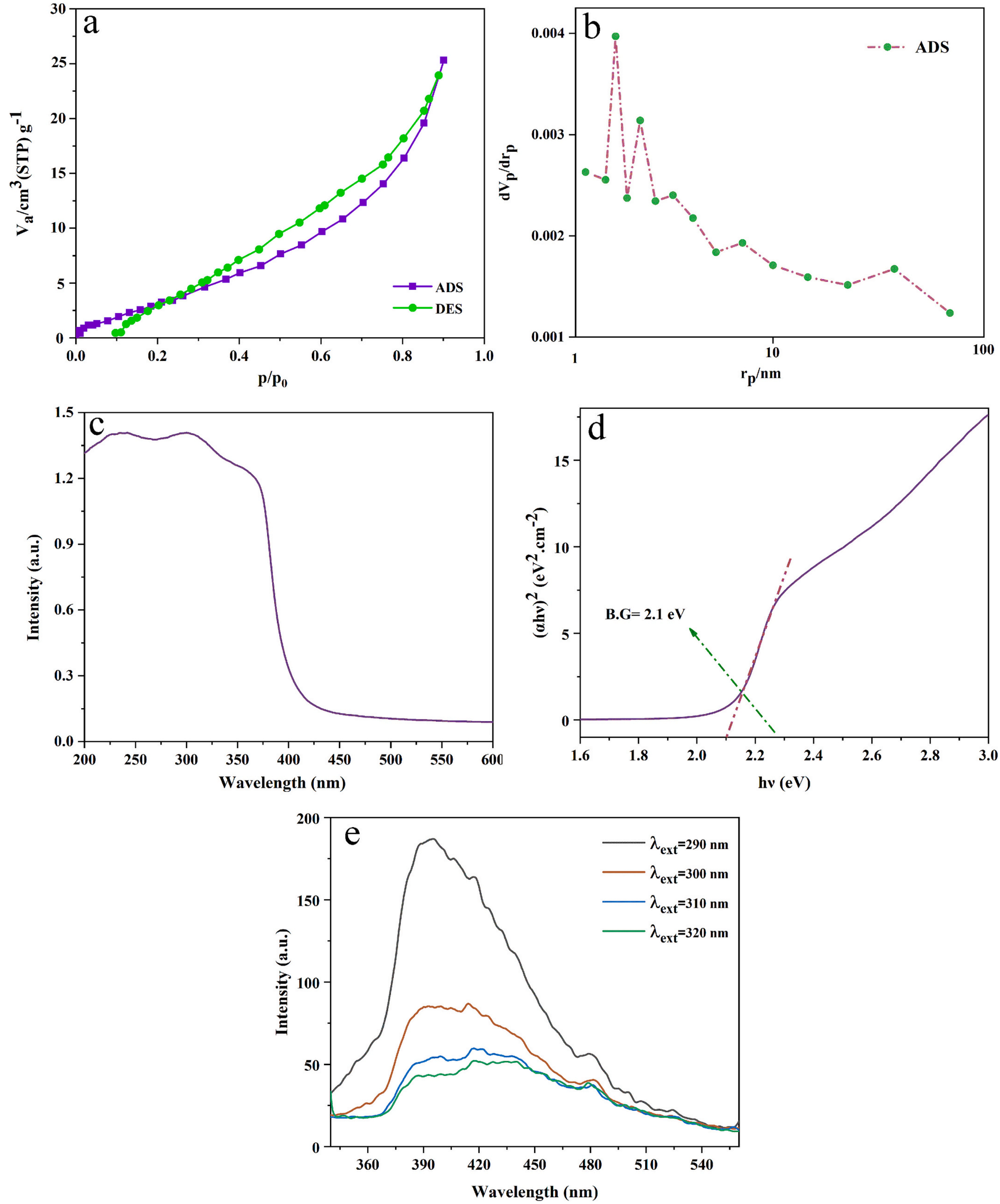

Fig. 4. a) N_2 adsorption-desorption isotherm, b) BJH plot, c)DRS spectrum, d)Tauc plot, and e) PL spetra of $Zn_2Ti_3O_8$ nanostructures.

Table 2
Frequency distribution of antibiotic resistance of *Klebsiella pneumoniae* isolates.

Antibiotics	Susceptible N (%)	Resistant N (%)
Ceftriaxone	0 (0)	44 (100)
Meropenem	0 (0)	44 (100)
Cefazolin	0 (0)	44 (100)
Cefotaxime	0 (0)	44 (100)
Cefalotin	0 (0)	44 (100)
Piperacillin / Tazobactam	0 (0)	44 (100)
Ampicillin	3 (6.81)	41 (93.18)
Aztreonam	4 (9.09)	40 (90.90)
Amikacin	6 (13.63)	38 (86.36)
Co-trimoxazole	6 (13.63)	38 (86.36)

Table 3
Distribution of MIC of zinc titanate nanoparticles, zinc oxide nanoparticles and titanium dioxide nanoparticles in ESBL and Non-ESBL isolates.

Compound/MIC	Concentrations	ESBLs (n %)	Non- ESBLs (n %)
Zinc titanate nanoparticles	156.25 μg/mL	19 (55.55)	6 (65.92)
	78.12 μg/mL	16 (44.44)	2 (27.21)
	39.06 μg/mL	_	1 (6.37)
Zinc oxide nanoparticles	1250 μg/mL	10 (29.2)	1 (6.95)
	625 μg/mL	25 (70.8)	5 (55.55)
	312.5 μg/mL	_	3 (37.5)
Titanium dioxide nanoparticles	1250 μg/mL	24 (69.76)	6 (67.45)
	625 μg/mL	11 (30.24)	2 (23.25)
	312.5 μg/mL	_	1 (9.3)

of toxicity of titanium dioxide and zinc oxide nanoparticles against food pathogens, with *Salmonella*, *Klebsiella*, and *Shigella* inhibition [29]. Reddy et al. in another study, assessed the antimicrobial effect of ZnO nanoparticles on *Klebsiella pneumoniae*, presenting a MIC value of 40 μg/mL. Previous data regarding the time-kill assay showed that *K. pneumoniae* was inhibited by 0.75 mM ZnO NPs after four hours based on standard growth curves [30]. This particular finding, when compared to the studies provided, depicts the influential role of the $Zn_2Ti_3O_8$ nanoparticles in mitigating the virulence effects of *Klebsiella pneumoniae* at lower concentrations in comparison to zinc oxide and titanium dioxide nanoparticles alone and can be attributed to the exceptional properties within the structure of these $Zn_2Ti_3O_8$ nanoparticles.

3.5. Inhibitory effect of nanoparticles on biofilm formation

The biofilm-forming ability of clinical isolates of ESBL and non-ESBL *Klebsiella pneumoniae* was evaluated. Strong biofilm formation was observed in 79.5 % of ESBL isolates and 20.5 % of non-MDR isolates, while only three non-ESBL isolates demonstrated weak biofilm-forming ability. $Zn_2Ti_3O_8$ nanoparticles significantly decreased the formation of biofilm. Treatment with $Zn_2Ti_3O_8$ nanoparticles led to a pronounced reduction in biofilm development at both MIC and sub-MIC concentrations. Statistical analysis confirmed that $Zn_2Ti_3O_8$ exhibited the most significant inhibitory effect ($P < 0.001$), highlighting its superior anti-biofilm activity relative to ZnO and TiO_2 nanoparticles. These results demonstrate that $Zn_2Ti_3O_8$ effectively inhibits the formation of biofilms by *K. pneumoniae*, while other nanoparticles have shown a relatively lower inhibition (Table 4). Kalhor et al. investigated the inhibitory effect of zinc oxide nanoparticles formulated using Leaf Extract of *Typha Latifolia* on Biofilm Gene Expression of Multidrug-Resistant *Klebsiella Pneumoniae* strains and found them to be a potential antimicrobial and anti-biofilm agent [18]. Though this study reported the anti-biofilm potential of the ZnO nanoparticles, these results achieved a significantly higher inhibition in biofilm formation by $Zn_2Ti_3O_8$ nanoparticles in terms of time and MIC.

Table 4
Percentage of biofilm inhibition in MIC and $\frac{1}{2}$ MIC concentrations of zinc titanate nanoparticles, zinc oxide nanoparticles and titanium dioxide nanoparticles.

Statistical index	In MIC concentration		
	Zinc titanate nanoparticles	Zinc oxide nanoparticles	Titanium dioxide nanoparticles
$\bar{X}$	69.39	40	45.25
SD	5.1	5.28	4.8
P-value	<0.001		
Statistical index	In $\frac{1}{2}$ MIC concentrations		
$\bar{X}$	55.48	30.02	39.44
SD	3.2	3.7	5.78
P-value	<0.001		

3.6. The effect of sub-MIC nanoparticles on gene expressions of mrkA

The effect of zinc-titanate nanoparticles on the expression of the mrkA gene in *Klebsiella pneumoniae* was evaluated at MIC and Sub-MIC concentrations using quantitative real-time PCR. Relative gene expression was calculated using the ΔΔCt method with 16 s rRNA as the internal control. At MIC concentrations, mrkA expression decreased significantly in all samples, with mean values of 32.98 ± 0.67 % for Sample1, 34.60 ± 2.11 % for Sample2, and 35.48 ± 0.92 % for Sample3. The overall mean reduction at MIC was 34.36 ± 1.63 %. At Sub-MIC concentrations, expression reductions were slightly lower, with 26.69 ± 0.85 %, 25.91 ± 1.08 %, and 30.97 ± 0.81 % for Samples 1, 2, and 3, respectively, resulting in an overall mean decrease of 27.86 ± 2.49 %. Statistical analysis using one-way ANOVA with Tukey's post hoc test confirmed that the downregulation of mrkA at both MIC and Sub-MIC concentrations was highly significant ($p < 0.001$) (Fig. 5). A study conducted in 2023 with the aim of investigating the effect of zinc oxide (ZnO) and titanium dioxide (TiO_2) nanoparticles on the formation of biofilm and persistent cells in *K. pneumoniae*. Real-time PCR results showed that the levels of mrkH and fimH decreased and the expression of luxS and mazF increased [31]. This study confirms the efficacy of zinc oxide and titanium dioxide nanoparticles in reducing biofilm-related genes and aligns with our results. Our results indicate that mrkA gene downregulation was more efficient by $Zn_2Ti_3O_8$ nanoparticles. When assessing the impact of zinc oxide nanoparticles on drug-resistant *Klebsiella pneumoniae*, a corresponding reduction of 8.5-fold and 9-fold in mrkA and fimA gene expression was reported [32]. This study targets the same gene as the present study and demonstrates that ZnO - nanoparticles significantly reduce mrkA gene expression. Nevertheless, the decrease demonstrated here by $Zn_2Ti_3O_8$ nanoparticles is much bigger.

3.7. MTT cell toxicity analysis after binary treatments

The effect of zinc-titanate nanoparticles on the viability of human dermal fibroblasts (HDFs) was assessed using the MTT assay. Cells were exposed to a range of nanoparticle concentrations from 19.53 to 1250 μg/mL. Viability was calculated as a percentage relative to untreated control cells. All experiments were conducted in triplicate, including both biological and technical replicates, and results are presented as mean ± SD. Significant cytotoxicity was observed only at the highest concentrations: 625 μg/mL (75.28 ± 6.90 %) and 1250 μg/mL (44.45 ± 0.40 %). At lower concentrations, including MIC and Sub-MIC levels, cell viability remained above 96–98 %, with minimal variation (SD 0.7–1.6 %). These findings indicate that zinc-titanate nanoparticles are highly biocompatible at concentrations effective against *Klebsiella pneumoniae*, supporting their potential for therapeutic applications (Fig. 6). The MTT and LDH assay of HEp-2 cells infected with wild-type bacteria in comparison to HEp-2 cells infected with ZnO nanoparticles demonstrated maximum cytotoxicity of ZnO nanoparticles against

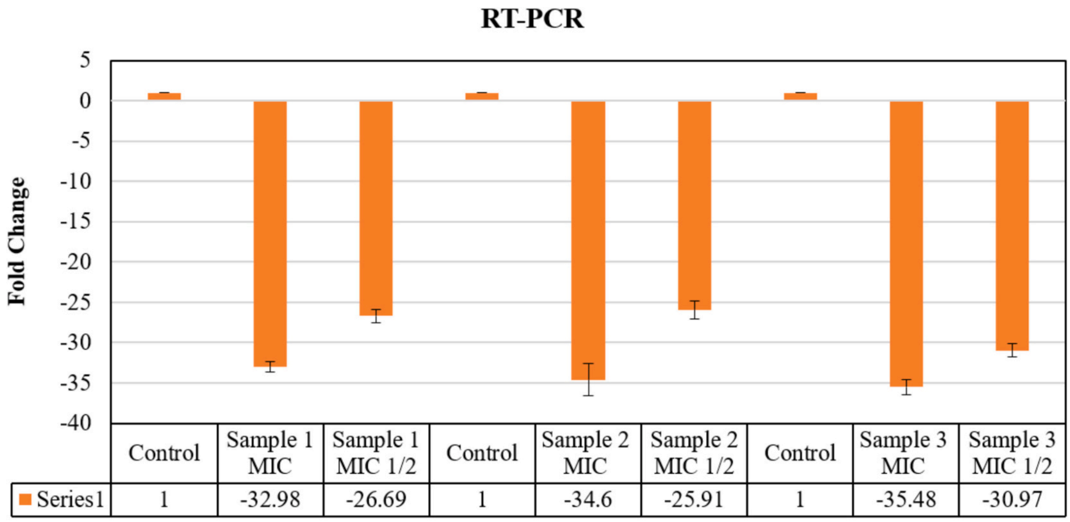

$\frac{1}{2}$

Fig. 5. Fold change of *Klebsiella pneumoniae* isolates treated with MIC and $\frac{1}{2}$ MIC of zinc titanate nanoparticles for the *mrkA* gene.

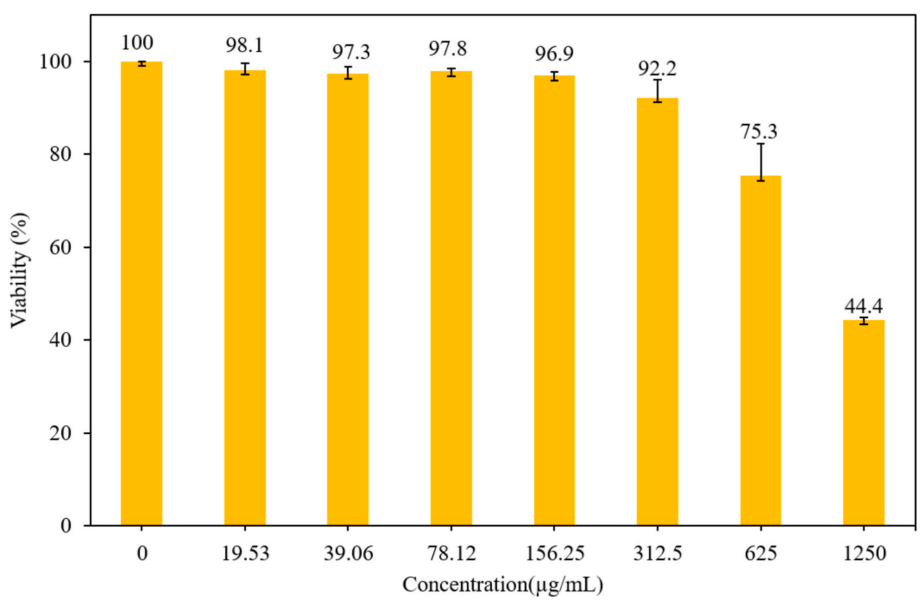

Fig. 6. Results of evaluating different concentrations $Zn_2Ti_3O_8$ nanoparticles on the viability of HDF cell line.

Klebsiella pneumoniae in the study; the cytotoxicity of ZnO was determined based on growth inhibition. In contrast, bacterial death by ZnO NPs at a dose of 0.50 mM and 0.75 mM was roughly 2.5 times less [30]. In another study that studied the synthesis, characterization, and evaluation of antimicrobial and cytotoxic effects of silver- and titanium-coated nanoparticles, they found that silver-coated nanoparticles (20–25 nm) had the best inhibition of tested microorganisms without cytotoxicity on the THP-1 monocytic cell lines [33]. While these studies support our findings, the cell line examined in this study was HDF rather than those used in these studies. The cytotoxic activity of $Zn_2Ti_3O_8$ nanoparticles was mild, restricted to concentrations above the MIC.

Table 5 shows the comparition study of $Zn_2Ti_3O_8$ with other similar compounds. Of the nanoparticles tested, $Zn_2Ti_3O_8$ had the best antibacterial and antibiofilm activity against *K. pneumoniae*; it had an extremely low MIC (39.06–156.25 µg/mL) compared with ZnO and TiO_2 (≥312.5 µg/mL). Overall, $Zn_2Ti_3O_8$ had the best biofilm inhibition at both MIC (69.39 %) and ½ MIC (55.48 %). $Zn_2Ti_3O_8$ was also very biocompatible, with at least 96 % cell viability in HDF cells. From gene expression analysis, we saw that the biofilm associated mrkA gene was down regulated, this demonstrated the antibiofilm activity of $Zn_2Ti_3O_8$ was associated with inhibition of the biofilm associated gene. ZnO, TiO_2, and $Cu_2Ti_2O_5$ all had very little activity with a high MIC value and biofilm inhibition percentages indicating that $Zn_2Ti_3O_8$ had great antibacterial and antibiofilm activity potential.

3.8. Photocatalytic activity

The photocatalytic activity of $Zn_2Ti_3O_8$ has been systematically studied under visible light for different organic dyes and experimental conditions, as exemplified in Fig. 7. Fig. 7a shows the degradation of various dyes, including methylene blue (MB), rhodamine B (RhB), and methyl orange (MO). Among the three dyes, MB had the highest dye

Table 5
The antibacterial and antibiofilm activities of different compounds.

Nanoparticle	Type of Bacteria	MIC (μg/mL)	Biofilm inhibition at MIC (%)	Biofilm inhibition at 1/2 MIC (%)	Cell viability at MIC (%)	Gene expression	Reference
$Zn_2Ti_3O_8$	*Klebsiella pneumoniae*	39.06–156.25	69.39	55.48	≥96 (at HDF Cells)	*mrkA* 33.40 (MIC) 28.93 (/½MIC) ↓	This study
ZnO	*Klebsiella pneumoniae*	312.5–1250	40.00	30.02	_	_	This study
TiO_2	*Klebsiella pneumoniae*	312.5–1250	45.25	39.44	_	_	This study
TiO_2	*Klebsiella pneumoniae*	2000	_	_	_	*gimH* (15 %) *K2A* (12.5 %) ↑	[38]
Cu_2Ti2O_5	*Klebsiella pneumoniae*	156.25–625	76	53.5	_	_	[39]
TiO_2	*Pseudomonas aeruginosa*	_	94	_	_	_	[40]
ZnO	*Pseudomonas aeruginosa*	8000	_		_	*maze, mqsA, higB* ↑	[41]
*TiO_2/MWCNTs **ZnO/ MWCNTs	*Escherichia coli* *Staphylococcus aureus*	*100 **100 *100 **1	_	_	–	_	[42]
TiO_2	*Pseudomonas aeruginosa (MDR clinical isolates)*	8–64	_	96	_	↓ *MexA*, *MexB* (~48–64 fold), *MexY* (~175 fold) ↓ *lasI*, *lasR*, *rhlI*, *rhlR*, *pqsA*, *pqsR* (~10–15 fold) slight ↑ *oprM*	[43]

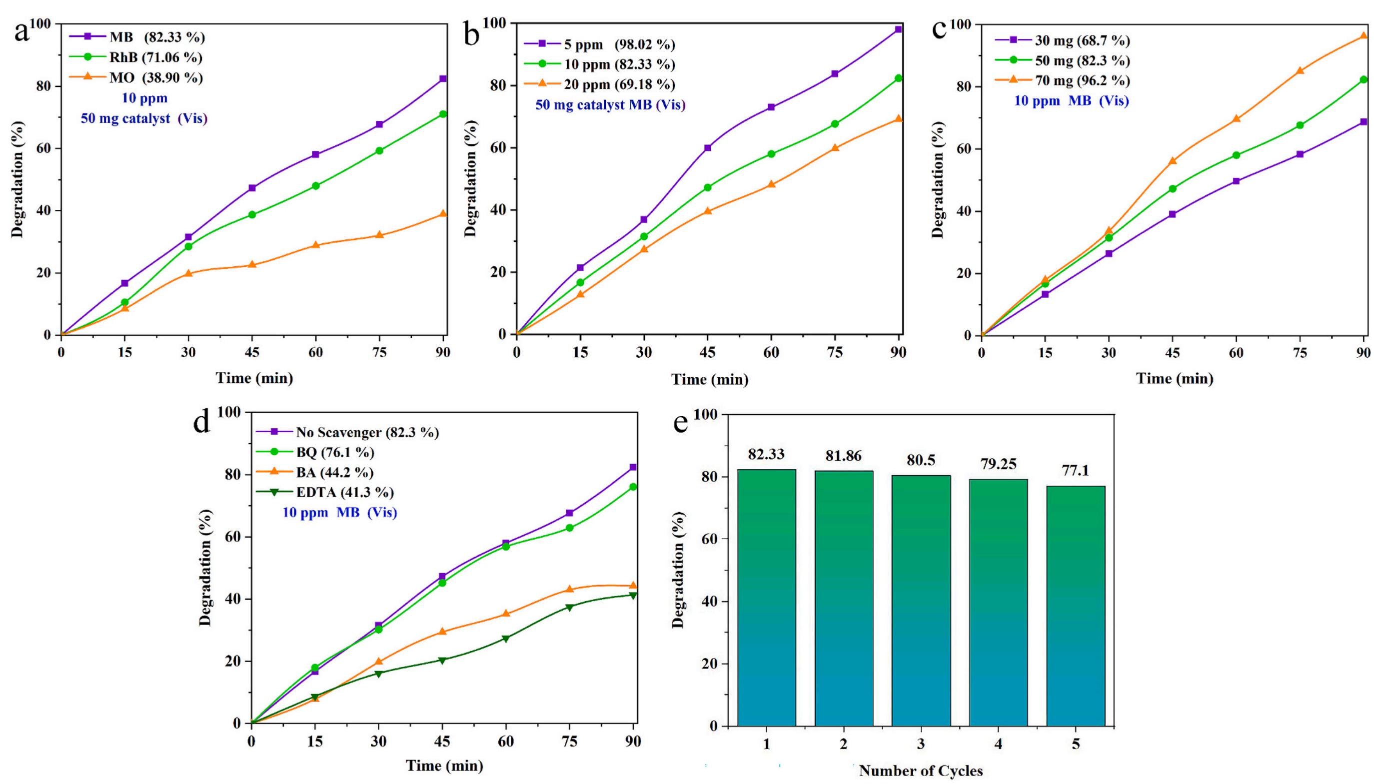

Fig. 7. Photocatalytic degradation of a) different dyes, b) different MB concentrations, c) different catalyst dosages, d) effect of scavengers, and e) recycleability test.

removal rate of 82.33 %, followed by RhB 71.06 %, and MO 38.90 %. This difference is ascribed to the molecular structure and adsorption mode of the dyes on the catalyst surface. The enhanced photocatalysis performance towards MB might be based on the higher adsorbability and electron transfer suitable ability of $Zn_2Ti_3O_8$ compared to MO. To investigate the effect of initial dye concentration, the degradation of MB at 5, 10, and 20 ppm was studied (Fig. 7b). It indicated a decrease in degradation efficiency with increasing concentration. The degradation percentages were 98.02 %, 82.33 %, and 69.18 % for 5 ppm, 10 ppm, and 20 ppm, respectively. On the other hand, this decrease is due to the small number of active sites on the surface of the catalyst and the increase in the light absorption of the dye itself at higher concentration, which can suppress the penetration of light and decrease the formation of reactive species. The influence of catalyst dosage was also studied by changing the quantity of $Zn_2Ti_3O_8$ catalyst from 30 to 70 mg at a constant MB concentration of 10 ppm (Fig. 7c). The degradation efficiency could be enhanced with catalyst dose and at 70 mg, the degradation efficiency was 96.2 % and it was observed to be 82.3 % and 68.7 % at 50 mg and 30 mg of catalyst usage, respectivley. This enhancement is attributed to the increased density of active sites for the photocatalytic reaction at higher catalyst concentrations. The aggregation or scattering of light may decrease the efficiency above an optimal amount. To determine the major reactive species in photocatalysis, scavenger experiments with benzoquinone (BQ) for superoxide radicals ($\cdot O_2^-$), benzoic acid (BA) for hydroxyl radicals (·OH), and EDTA for photogenerated holes (h^+) were performed (Fig. 7d). The degradation efficiency decreased significantly with BA (44.2 %) and EDTA (41.3 %) compared to the control(82.3 %), suggesting that both ·OH and h^+ are predominant in the degradation process. The slight decrease with BQ (76.1 %) suggests that $\cdot O_2^-$ is also involved, but less so. Lastly, the recyclability of the $Zn_2Ti_3O_8$ photocatalyst was evaluated for five successive cycles based on MB degradation under visible light (Fig. 7e). The catalyst kept a majority of its activity with minimal decline in efficiency from 82.33 % in the first cycle to 77.1 % in the fifth cycle, which illustrates good durability and stability of the material upon successive applications. In general, these findings prove that $Zn_2Ti_3O_8$ is a good and reusable visible-light-driven photocatalyst, especially for MB degradation. The photocatalytic activity is highly dependent on dye type, initial dye concentration, catalyst dosage, and the role of reactive oxygen species. These results demonstrate the practicality of $Zn_2Ti_3O_8$ for wastewater treatment applications.

To acquire more information regarding the reaction mechanism, the photocatalytic degradation kinetics of methylene blue (MB) over $Zn_2Ti_3O_8$ under visible light illumination was examined based on a pseudo-first-order kinetic model commonly employed in heterogeneous photocatalysis. The kinetic parameters are presented in Fig. 8. According to the model, the rate of degradation follows the Eq. [34]:

$$\ln(C_0/C) = kt \quad (4)$$

where C_0 is the initial concentration of the dye, C is the concentration at time t, and k is the apparent rate constant. The linear correlations between $\ln(C_0/C)$ and time for MB degradation indicate a good fit, indicating the suitability of the pseudo-first-order model for this system. The slope of each line is equal to the rate constant (k) and is a measure of the rate of photocatalytic reaction under prevailing conditions. It can be observed from the kinetic constants determined that the $Zn_2Ti_3O_8$ catalyst allows for a relatively fast degradation of MB under visible light, which is in agreement with the high percentages of degradation observed in Fig. 8. This kinetic study reconfirms earlier results that $Zn_2Ti_3O_8$ is an efficient photocatalyst for decolorization of MB and that surface-mediated redox processes, through the photogenerated holes and electrons, control the catalytic activity. The evidence from kinetics combined with that obtained from the scavenger test provides more insight into the degradation mechanism and reasserts the practical

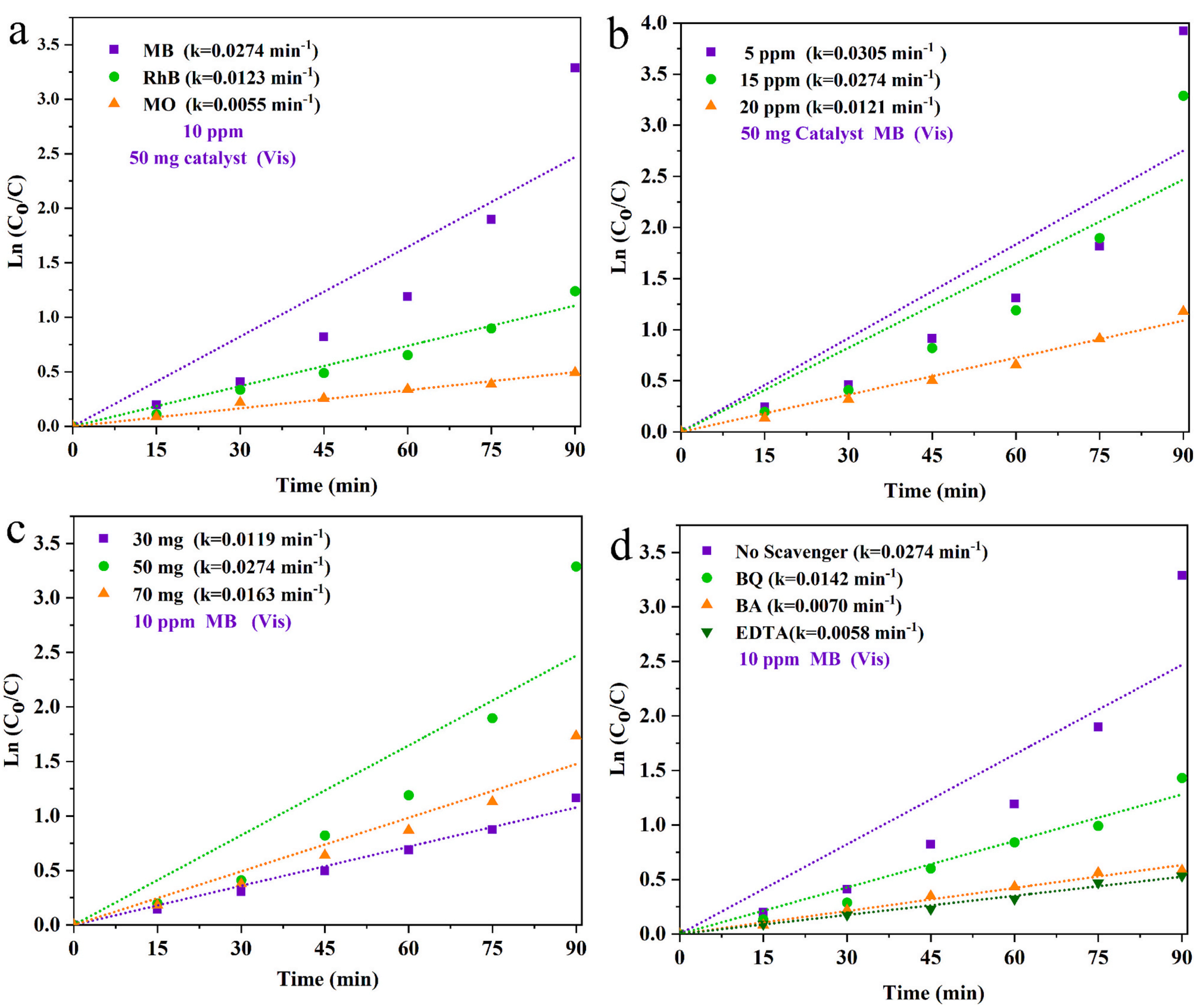

Fig. 8. Kinetics study of a) different dyes, b) different MB concentrations, c) different catalyst dosages, d) effect of scavengers.

feasibility of the material for wastewater treatment.

The research on $Fe_3O_4@SiO_2$/Schiff-Base/Zn(II) nanoparticles clearly indicates that hybrid nanostructures can provide multifunctional potential and show robust antimicrobial efficacy [35], relating back to our work where we designed $Zn_2Ti_3O_8$ with antimicrobial and photocatalytic properties. Equally, studies on MXenes, which act as versatile agents against microorganisms, also highlight the necessity of novel materials that provide broad-spectrum activity benefits through unique structural and electronic properties [36], emphasizing further the novelty of using $Zn_2Ti_3O_8$ as a multifunctional alternative. The other work reviewing methylene blue adsorption with activated carbon emphasizes that kinetics and mechanistic studies are crucial for validating adsorption vs. degradation pathways [37]. This complements our survey on photocatalytic degradation, where we quantitatively measured the dye degradation rate, linked this observation to bandgap properties, and compared performance benchmarks with other performance reports on titanates. By setting our study in context, we have clarified the primary argument of our study, which is to showcase $Zn_2Ti_3O_8$ nanoparticles as a new class of multifunctional material that can promote effective antibacterial/antibiofilm activity, as well as visible-light photocatalysis. The results add to an ever-growing body of work to develop next-generation nanomaterials with broad applicability within biomedical and environmental applications. Table 6 reveals the photocatalytic comparison study of different orthotitanate compounds. The photocatalytic findings support that $Zn_2Ti_3O_8$ is an efficient catalyst triggered by visible light. $Zn_2Ti_3O_8$ (bandgap ~2.1 eV) achieved 96.2 % degradation of methylene blue in visible light in 90 min, which is greater than most of the different orthotitanates and nanocomposites. For instance, $SrTiO_3$ and TiO_2/ZnO composites exhibited only moderate degradation with 64–94 % and even an ~72.34 % degradation, eventually needing greater dosage or stronger light sources. While the other bimetallic mixed phase, $NiTiO_3$, and Zn_2TiO_4/g-C_3N_4 hardly provided any efficiency (≤46 % efficiency). This just demonstrates that $Zn_2Ti_3O_8$ combines a bandgap small enough to have visible-light activation and also has, importantly, more exceptional photocatalytic performance under mild conditions.

4. Conclusions

To sum up, we have prepared $Zn_2Ti_3O_8$ nanoparticles through a simple and inexpensive Pechini route and demonstrated the materials' multifunctional performance. When compared to either ZnO or TiO_2 nanoparticles, the significantly lower MIC of $Zn_2Ti_3O_8$ for *Klebsiella pneumoniae* (39.06 μg/mL contrasted with >100 μg/mL typically reported for ZnO/TiO_2) demonstrated much of its superior antibacterial performance. In addition to growth inhibition, we also demonstrated that $Zn_2Ti_3O_8$ reduced biofilm formation with a maximum with of 69.39 % at MIC and 55.48 % at ½ MIC and significantly downregulated the mrkA gene (33.03 % and 28.52 % at MIC and ½ MIC, respectively); this establishes novelty for $Zn_2Ti_3O_8$ as a dual-function bactericidal agent that kills bacteria and inhibits biofilm-associated virulence. Testing our material for cytotoxicity at effective antimicrobial doses also demonstrated acceptable biocompatibility since cytotoxicity was only observed at comparatively high $Zn_2Ti_3O_8$ doses. These results suggest that $Zn_2Ti_3O_8$ is a viable option for infection control (especially against biofilm forming, multi-drug resistant pathogens) and for wastewater treatment. Future tests using broader microbial panels, as well as in real wastewater systems will confirm real-world applicability and scalability. Additionally, $Zn_2Ti_3O_8$ demonstrated very strong photocatalytic activity, with 98.02 % methylene blue degradation after 90 min of visible light exposure. The catalyst also was not visibly degraded through repeated cycles and was would appear to exhibit stability for further application. The combination of strong antibacterial, anti-biofilm, and photocatalytic materials into a single nanomaterial clearly has a value-added scientific implication, giving a unique connection between biomedical and environmental applications. The results suggest that $Zn_2Ti_3O_8$ would be an excellent candidate for the dual applications of infection control (especially with multidrug-resistant, biofilm-forming pathogens) and wastewater treatment. The next steps will be to broaden microorganism beyond *E coli*, Staphylococcus, and Pseudomonas, and to see how the material performs with real wastewater.

CRediT authorship contribution statement

Mohammad Reza Saadati-Gullojeh: Validation, Software, Methodology, Investigation, Formal analysis, Data curation. **Matin Valipour Motlagh:** Software, Resources, Methodology, Investigation, Formal analysis, Data curation. **Mojgan Ghanbari:** Writing – review & editing, Writing – original draft, Visualization, Validation, Supervision. **Amar Yasser Jassim:** Writing – review & editing, Software, Resources. **Forat H. Alsultany:** Writing – review & editing, Software, Resources. **Ayad F. Alkaim:** Writing – review & editing, Software, Resources. **Masoud Salavati-Niasari:** Writing – review & editing, Writing – original draft, Visualization, Validation, Supervision, Software, Resources, Project administration, Methodology, Investigation, Funding acquisition, Formal analysis, Data curation, Conceptualization. **Azad Khaledi:** Validation, Software, Resources.

Ethics statement

The current study has received ethical authorization from the Ethics Committee of Kashan University of Medical Sciences, Kashan, Iran (IR.KAUMS.MEDNT.REC.1402.165).

Funding

This study was financially supported by the Vice-Chancellor of Research, Kashan University of Medical Sciences, Kashan, Iran [Grant number: 402106] and the council of the Iran National Science Foundation, INSF (4041658), and the University of Kashan for supporting this work through Grant No. 159271/FU1P.

Declaration of competing interest

The authors declare that they have no known competing financial

Table 6
The photocatalytic performance of different ortho titanate compounds.

Catalyst	Bandgap (eV)	Solution pH	Highest degradation (%)	Dye concentration (ppm)	Catalyst dosage (g/L)	Source of light/Time (min)	Ref.
$Zn_2Ti_3O_8$	2.1	7	96.2 (MB)	10	0.07	Vis /90	This work
$Zn_2Ti_3O_8$	1.8	7	70.0 (RhB)	10	0.05	Vis /90	[18]
Zn_2TiO_4/g-C_3N_4	2.8	7	46.2 (MB)	5	0.5	UV/120	[44]
C_3N_4-ZnO-$Zn_2Ti_3O_8$	3.11	6–7	82–99 (MB)	5	0.2	UV/45	[45]
TiO_2/ZnO nanocomposite	3.3	–	72.34 (MB)	10	0.1	Vis/ 60	[46]
$SrTiO_3$	2.43–2.57	–	64–94 (MB)	10	0.05	500 W halogen lamp /90	[47]
$NiTiO_3$	2.5	–	42 (MB)	10	0.05	Vis /180	[48]

interests or personal relationships that could have appeared to influence the work reported in this paper.

Acknowledgments

The authors would like to thank the Clinical Research Development Unit of Kashan Shahid Beheshti Hospital in Kashan University Medical Sciences.

Data availability

The authors do not have permission to share data.

References

[1] Y.R. Saharman, A. Karuniawati, J.A. Severin, H.A. Verbrugh, Infections and antimicrobial resistance in intensive care units in lower-middle income countries: a scoping review, Antimicrobial Resistance & Infection, Control 10 (2021) 1–19.
[2] R. Mirghani, T. Saba, H. Khaliq, J. Mitchell, L. Do, L. Chambi, K. Diaz, T. Kennedy, K. Alkassab, T. Huynh, Biofilms: Formation, drug resistance and alternatives to conventional approaches, AIMS microbiology 8 (2022) 239.
[3] H. Jiang, L. Li, Z. Li, X. Chu, Metal-based nanoparticles in antibacterial application in biomedical field: Current development and potential mechanisms, Biomed. Microdevices 26 (2024) 12.
[4] F.I. Abou El Fadl, D.E. Hegazy, N.A. Maziad, M.M. Ghobashy, Effect of nano-metal oxides (TiO2, MgO, CaO, and ZnO) on antibacterial property of (PEO/PEC-co-AAm) hydrogel synthesized by gamma irradiation, Int. J. Biol. Macromol. 250 (2023) 126248.
[5] K. Skłodowski, S.J. Chmielewska-Deptuła, E. Piktel, P. Wolak, T. Wollny, R. Bucki, Metallic nanosystems in the development of antimicrobial strategies with high antimicrobial activity and high biocompatibility, Int. J. Mol. Sci. 24 (2023) 2104.
[6] S. Fatima, K. Ali, B. Ahmed, A.A. Al Kheraif, A. Syed, A.M. Elgorban, J. Musarrat, J. Lee, Titanium dioxide nanoparticles Induce inhibitory effects against planktonic cells and biofilms of human oral cavity isolates of Rothia mucilaginosa, Georgenia sp. and Staphylococcus saprophyticus, Pharmaceutics 13 (2021) 1564.
[7] S. Ghosh, A. Das, Modified titanium oxide (TiO2) nanocomposites and its array of applications: a review, Toxicol. Environ. Chem. 97 (2015) 491–514.
[8] S. Rashki, E.A. Dawi, M.R. Zilaei, H. Safardoust-Hojaghan, M. Ghanbari, A. Ryadh, H.A. Lafta, A. Khaledi, M. Salavati-Niasari, ZnO/chitosan nanocomposites as a new approach for delivery LL37 and evaluation of the inhibitory effects against biofilm-producing Methicillin-resistant Staphylococcus aureus isolated from clinical samples, Int. J. Biol. Macromol. 253 (2023) 127583.
[9] V. Ageh, H. Mohseni, T.W. Scharf, Lubricious zinc titanate coatings for high temperature applications, Surf. Coat. Technol. 237 (2013) 241–247.
[10] Y.-L. Huang, D.-C. Tsai, Y.-C. Lee, D.-R. Jung, F.-S. Shieu, Effect of annealing on microstructure and dielectric properties of Zn2Ti3O8 thin films by reactive co-sputtering, Surf. Coat. Technol. 231 (2013) 153–156.
[11] N.K. Pandey, K. Tiwari, A. Roy, ZnO–TiO2nanocomposite: Characterization and moisture sensing studies, Bull. Mater. Sci. 35 (2012) 347–352.
[12] B.C. Yadav, A. Yadav, S. Singh, K. Singh, Nanocrystalline zinc titanate synthesized via physicochemical route and its application as liquefied petroleum gas sensor, Sensors Actuators B Chem. 177 (2013) 605–611.
[13] A. Stoyanova, H. Hitkova, A. Bachvarova-Nedelcheva, R. Iordanova, N. Ivanova, M. Sredkova, Synthesis, photocatalytic and antibacterial properties of nanosized ZnTiO3 powders obtained by different sol-gel methods, Digest Journal of Nanomaterials and Biostructures 7 (2012) 777–784.
[14] K.M. Lee, C.W. Lai, K.S. Ngai, J.C. Juan, Recent developments of zinc oxide based photocatalyst in water treatment technology: a review, Water Res. 88 (2016) 428–448.
[15] Q. Guo, C. Zhou, Z. Ma, X. Yang, Fundamentals of TiO2 photocatalysis: concepts, mechanisms, and challenges, Adv. Mater. 31 (2019) 1901997.
[16] N.M. Vaziri, S. Salehipour, Performance of Lightweight alkali-activated slag concrete before and after exposure to elevated temperatures: mechanical properties and durability, J. Build. Eng. 112 (2025) 113907.
[17] L. Zhang, J. Zhang, H. Yu, J. Yu, Emerging S-scheme photocatalyst, Adv. Mater. 34 (2022) 2107668.
[18] M.R. Saadati-Gullojeh, M. Ghanbari, M. Salavati-Niasari, Facile preparation and characterization of Zn2Ti3O8/g-C3N4 nanocomposites for degradation of rhodamine B under simulated sunlight, Sol. Energy 268 (2024) 112316.
[19] M. Mojaddarasil, M.R. Tavakoli, Investigation of Polyamide 12 Powder Cooling Process under Natural Convection via Porous Medium, Non-porous Medium, and Experimental Approaches, J. Mater. Eng. Perform. 34 (2025) 9352–9373.
[20] S. Rashki, M. Ghanbari, Z.H. Khudhair, Z. Marzhoseyni, Z. Bameri, S. Afsharikhah, W.K. Abdulsahib, A. Nazari-Alam, M. Salavati-Niasari, Evaluate the effect of graphitic carbon nitride nanosheets decorated with copper nanoparticles on biofilm and icaA gene expression in Staphylococcus aureus isolated from clinical samples, Arab. J. Chem. 16 (2023) 104882.
[21] M.P. Weinstein, J.S. Lewis, The clinical and laboratory standards institute subcommittee on antimicrobial susceptibility testing: background, organization, functions, and processes, J. Clin. Microbiol. 58 (2020), https://doi.org/10.1128/jcm. 01864-01819.
[22] M. Rahimi, A. Piroozmand, M. Shayestehpour, S. Salamat, F. Peik Falak, A. Shakerimoghaddam, G.A. Moosavi, A. Khaledi, Effect of curcumin nanoparticles and alcoholic extract of Falcaria vulgaris on the growth rate, biofilm, and gene expression in Pseudomonas aeruginosa isolated from burn wound infection, Mol. Biol. Rep. 50 (2023) 6681–6690.
[23] V. Arulmozhi, K. Pandian, S. Mirunalini, Ellagic acid encapsulated chitosan nanoparticles for drug delivery system in human oral cancer cell line (KB), Colloids Surf. B: Biointerfaces 110 (2013) 313–320.
[24] M.R. Saadati-Gullojeh, M. Ghanbari, A. Ehsani, F.H. Alsultany, H.H. Hamza, M. Salavati-Niasari, Pechini synthesis and characterization of Ni3TiO5/NiTiO3 nanocomposites and their application as nano-photocatalyst for degradation of water-soluble organic pollutants under visible light, Surf Interfaces 66 (2025) 106604.
[25] R.B. Pinto, P. Peralta-Zamora, F. Wypych, Fabrication of ZnO-Zn2TiO4 nanocomposite from zinc hydroxide nitrate and its photocatalytic efficiency, J. Photochem. Photobiol. A Chem. 353 (2018) 46–52.
[26] M.R. Saadati-Gullojeh, M. Salavati-Niasari, M. Ghanbari, A. Ehsani, Supercapacitor, electrochemical measurement and sun light driven nano-photocatalytic applications of Co2TiO4/CoTiO3 nanocomposites synthesized from Pechini sol-gel method, Results in Engineering 25 (2025) 103846.
[27] K.T.A. Priyangga, Y.S. Kurniawan, L. Yuliati, High photocatalytic activity of zinc metatitanate materials for phenol photodegradation, IOP Conference Series: Materials Science and Engineering 1143 (2021) 012076.
[28] M. Mohammadi, D. Fray, Low temperature nanostructured zinc titanate by an aqueous particulate sol–gel route: optimisation of heat treatment condition based on Zn: Ti molar ratio, J. Eur. Ceram. Soc. 30 (2010) 947–961.
[29] G.D. Venkatasubbu, R. Baskar, T. Anusuya, C.A. Seshan, R. Chelliah, Toxicity mechanism of titanium dioxide and zinc oxide nanoparticles against food pathogens, Colloids Surf. B: Biointerfaces 148 (2016) 600–606.
[30] L.S. Reddy, M.M. Nisha, M. Joice, P. Shilpa, Antimicrobial activity of zinc oxide (ZnO) nanoparticle against Klebsiella pneumoniae, Pharm. Biol. 52 (2014) 1388–1397.
[31] A. Pourmehdiabadi, M.S. Nobakht, B. Hajjam Balajorshari, M.R. Yazdi, K. Amini, Investigating the effects of zinc oxide and titanium dioxide nanoparticles on the formation of biofilm and persister cells in Klebsiella pneumoniae, J. Basic Microbiol. 64 (2024) 2300454.
[32] A. Shivaee, S.K. Kashani, R. Mohammadzadeh, M.T. Ebrahimi, Effect of Zinc Oxide Nanoparticle on the Expression of mrkA and fimA in Drug-Resistant Klebsiella pneumoniae, Journal of Medical Bacteriology (2021) 1–10.
[33] F. Martinez-Gutierrez, P.L. Olive, A. Banuelos, E. Orrantia, N. Nino, E.M. Sanchez, F. Ruiz, H. Bach, Y. Av-Gay, Synthesis, characterization, and evaluation of antimicrobial and cytotoxic effect of silver and titanium nanoparticles, Nanomedicine: Nanotechnology, Biology and Medicine 6 (2010) 681–688.
[34] M. Hosseini, M. Ghanbari, E.A. Dawi, M.A. Mahdi, S.H. Ganduh, L.S. Jasim, A.M. M. Ibrahim, M. Salavati-Niasari, Investigations of nickel silicate for degradation of water-soluble organic pollutants, Int. J. Hydrog. Energy 61 (2024) 307–315.
[35] S. Azadi, A.M. Amani, A. Jangjou, A. Vaez, Z. Zareshahrabadi, A. Zare, S.R. Kasaee, H. Kamyab, S. Chelliapan, S. Mosleh-Shirazi, Fe3O4@SiO2/Schiff-base/Zn (II) nanocomposite functioning as a versatile antimicrobial agent against bacterial and fungal pathogens, Sci. Rep. 15 (2025) 5694.
[36] A.M. Amani, A. Rahbar, E. Vafa, L. Tayebi, M. Abbasi, H. Kamyab, S. Chelliapan, S. R. Kasaee, A. Vaez, S. Mosleh-Shirazi, Exploring the functionality of MXenes as promising versatile antimicrobial agents and their novel applications, Mater Today Commun 41 (2024) 110774.
[37] S.T. Al-Asadi, Z.H. Mussa, F.F. Al-Qaim, H. Kamyab, H.F.S. Al-Saedi, I.F. Deyab, N. J. Kadhim, A comprehensive review of methylene blue dye adsorption on activated carbon from edible fruit seeds: A case study on kinetics and adsorption models, Carbon Trends 20 (2025) 100507.
[38] A. Al-Najim, A. Hamid, A. Basheer, F. Mahmood, E. Hasan, Effect of nanoparticles on the expression of virulence and biofilm genes in Klebsiella pneumoniae, Regulatory Mechanisms in Biosystems 15 (2024) 826–829.
[39] M. Poudineh, M. Valian, A.Y. Jassim, Z. Ghorbani, A. Khaledi, M. Salavati-Niasari, Synthesis, characterization, and biomedical applications (antibacterial, antibiofilm, anticancer and effects on hospital-acquired pneumonia infection) of copper titanium oxide nanostructures, RSC Adv. 15 (2025) 5124–5134.
[40] S.H. Haji, A.R. Ganjo, T.A. Faraj, M.H. Fatah, S.B. Smail, The enhanced antibacterial and antibiofilm properties of titanium dioxide nanoparticles biosynthesized by multidrug-resistant Pseudomonas aeruginosa, BMC Microbiol. 24 (2024) 379.
[41] H. Valadbeigi, N. Sadeghifard, V.H. Kaviar, M.H. Haddadi, S. Ghafourian, A. Maleki, Effect of ZnO nanoparticles on biofilm formation and gene expression of the toxin-antitoxin system in clinical isolates of Pseudomonas aeruginosa, Ann. Clin. Microbiol. Antimicrob. 22 (2023) 89.
[42] S. Shafique, Z. Khalid, S. Arif, Z. Noreen, L. Tabassam, M. Waseem, ZnO, TiO_2 and Ag_2O decorated MWCNTs for enhanced antibacterial and antidiabetic activities, Inorg. Chem. Commun. 163 (2024) 112383.
[43] F.Y. Ahmed, U.F. Aly, R.M. Abd El-Baky, N.G. Waly, Effect of titanium dioxide nanoparticles on the expression of efflux pump and quorum-sensing genes in MDR Pseudomonas aeruginosa isolates, Antibiotics 10 (2021) 625.
[44] Ö. Tuna, E.B. Simsek, Construction of novel Zn2TiO4/g-C3N4 Heterojunction with efficient photodegradation performance of tetracycline under visible light irradiation, Environ. Sci. Pollut. Res. 28 (2021) 10005–10017.
[45] N. Sutanto, K.A. Saharudin, S. Sreekantan, V. Kumaravel, H. Md Akil, Heterojunction catalysts g-C3N4/-3ZnO-c-Zn2Ti3O8 with highly enhanced visible-light-driven photocatalytic activity, J. Sol-Gel Sci. Technol. 93 (2020) 354–370.

[46] L. Wang, X. Fu, Y. Han, E. Chang, H. Wu, H. Wang, K. Li, X. Qi, Preparation, characterization, and photocatalytic activity of TiO2/ZnO nanocomposites, J. Nanomater. 2013 (2013) 321459.
[47] S. Neti, A.R. Nanmangalam, C.N. Chintakuntla, T. Ramasamy, S. Sankaranarayanan, Structural influence of strontium titanate nanocubes for photocatalytic dye degradation and electrochemical applications, Inorg. Chem. Commun. 148 (2023) 110299.
[48] S. Subramanian, S. Ganapathy, S. Subramanian, T. Ramasamy, J. Ramasamy, Enhancement in visible light photocatalytic performance using silver-decorated nickel titanate nanofiber composite, Inorg. Chem. Commun. 132 (2021) 108821.

Mohammad Reza Saadati-Gullojeh received her bachelor's degree in chemistry from the Farhangian Teacher Education University (FTEU) and his master's degree in Nano chemistry from University of Zanjan (ZNU). Currently, he is a PhD candidate in Nano chemistry at the University of Kashan, Iran. His main research focuses on the synthesis, characterization and investigation of optical and electrochemical properties of Titanate-based perovskite and nanocomposite with Graphitic carbon nitride structures (g-C_3N_5 and g-C_3N_4) and their application energy storage in supercapacitor systems and photocatalytic processes.

Matin Valipour Motlagh received his bachelor's degree in microbiology from Isfahan University of Iran (UOI). Currently, he is a master's candidate in medical microbiology at Kashan University of Medical Sciences. His main research focuses on "Inhibition of pathogenesis with nanoparticles such as Zn and Ti and applications of Probiotics." His article discusses the growth of resistant microbes with the aid of nanoparticles. He's also working on AI training to use in his next articles related to the effect of nanoparticles and antibiotics on bacteria, cancer detection using miRNA biomarkers, cancer treatment using nanoparticles, and diagnosing about 80% of the diseases.

Mojgan Ghanbari received her PhD from the Institute of Nano Science and Nano Technology, University of Kashan, Iran, and is presently a postdoctoral researcher. Her research interests primarily include the fabrication and application of novel nanostructured materials for water contamination remediation, photocatalysis, tissue engineering, and the development of novel formulations for pharmaceutical hard capsules. She is an active researcher with over 68 ISI-indexed publications in high-quality journals, and her scientific endeavors have earned her a place among the top 2% of scientists worldwide in recent years. As an aside to her research commitment, here is further evidence of the extent of her contribution to inorganic and materials chemistry—Dr. Ghanbari's involvement as a reviewer for many peer-reviewed international journals.

Amar Yasser Jassim is a lecturer in the Marine Science Center at the University of Basrah (Iraq). He earned a PhD in environmental health sciences at the University of South Carolina (USA). His current research interest is in the biosynthesis of engineered nanoparticles and their application as antimicrobial agent together with understanding their environmental health and safety.

Forat H. Alsultany received the M.Sc. in Applied Physics (solid state) at the University Sciences Malaysia (USM) in 2014 and a PhD from Universiti Sains Malaysia (USM), Malaysia, in 2017. The field of PhD study was: Materials Fabrication and Characterization for Optoelectronics and Biomedicine. He has published more than 100 papers in international journals. His work has been presented more than 14 international conferences as invited speaker

Ayad Alkaim is a PhD candidate in Chemistry at Babylon University in Hilla (Iraq). He obtained both his Master (2005) in Chemistry at Babylon University and a PhD (2011) degree in Chemistry at Babylon University supported by researchers scholarship in Hannover University, (Germany) working with Prof. Bahnemann's group). Alkaim research interests focus on the synthesis and nanomaterials (ZnO, TiO2), also hydrogel surfaces, and Adsorption locator by MD for applications in environmental catalysis, specifically the adsorption and photocatalytic degradation. He is an author and co-author in about 60 papers published in JCR.

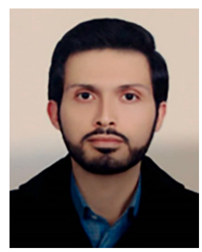

Mohammad Reza Rahimi received his bachelor's degree in laboratory science from Islamic Azad University and his master's degree in medical microbiology from Kashan University of Medical Sciences (KAUMS). Currently, he is conducting his research activities at Kashan University of Medical Sciences. His main research interests focus on investigating the antimicrobial effects of nanoparticles, plant extracts, and various probiotics against pathogenic bacteria. His studies aim to investigate novel strategies to inhibit bacterial growth, with potential applications in the development of alternative antimicrobial agents and improving infection control approaches.

Masoud Salavati-Niasari is professor in Department of inorganic chemistry and Institute of Nano Science and Nano Technology at University of Kashan, Iran. He received his BSc degree in chemistry from Isfahan University in 1992, his MSc degree in inorganic chemistry from Isfahan University of Technology in 1995, and his Ph. D in inorganic chemistry from Tehran University, Iran, in 2001. His research covers heterogeneous & homogeneous catalysis, synthesis and characterization of coordination compounds, synthesis and characterization of nanostructures/nanocomposite materials, host guest chemistry, polymeric nanocomposite materials, solar cell, nano-biomaterials, nano-superconductors, flame retardant nanocomposite materials, nano-photocatalyst, electrochemical sensors, and energy storage. With a prolific research career, Masoud Salavati-Niasari has a prolific research output, having published a total of 1178 articles and over 60,113 citations (h = 144).

Azad Khaledi is a medical microbiologist, associate professor, and researcher at the Department of Microbiology, Faculty of Medicine, Kashan University of Medical Sciences, Iran. He has been working on various aspects of microbiology for several years, such as bacterial resistance, designing various types of antimicrobial agents, such as nanoparticles, peptides, and vaccines, and has collaborated with numerous scientists and reputable international centers in this regard.